internal energies. These effects are not well understood at this time.

We conclude that the metastable ion method and its results, as described above, provide an effective technique for studying the decomposition of reaction intermediates which could not be observed directly in the ICR cell. To the extent that isotope distributions probe the properties of the respective ions, the metastable ions generated at higher pressure have been shown to exhibit the same properties as reaction intermediates unobserved at low (ICR) pressures. This combination of techniques, including the labeling studies, reveals that the benzyl and tropylium ions formed most probably result from $C_9H_{11}^+$ species of structures I and II, respectively. Protonated aromatic species formed in the competing ion-molecule reaction result from simple proton transfer.

Acknowledgments. The authors are grateful to the National Science Foundation for support of this research through Grants GP 33870X and GP38125X. R.H. thanks the Fonds National Suisse for partial support. T.A.E. gratefully acknowledges support from the National Center for Toxicological Research. We are indebted to Professor T. Gäumann (EPF-Lausanne) for his generous gift of the 1-bromo[2-^{13}C]heptane.

References and Notes

(1) (a) Institut de Chimie Physique EPFL; (b) University of Utah.
(2) (a) H. M. Grubb and S. Meyerson in "Mass Spectrometry of Organic Ions", F. W. McLafferty, Ed., Academic Press, New York, N.Y., 1963, pp 516–519; (b) J. T. Bursey, M. M. Bursey, and D. G. I. Kingston, *Chem. Rev.*, **73**, 191 (1973); (c) F. W. McLafferty and J. Winkler, *J. Am. Chem. Soc.*, **96**, 5182 (1974); (d) L. P. Theard and W. H. Hamill, *ibid.*, **84**, 1134 (1962).
(3) R. P. Clow and J. H. Futrell, *J. Am. Chem. Soc.*, **94**, 3748 (1972).
(4) R. P. Clow and T. O. Tiernan, 21st Annual Conference on Mass Spectrometry and Allied Topics, San Francisco, Calif., May 20–25, 1973, Paper B-4.
(5) M. S. B. Munson and F. H. Field, *J. Am. Chem. Soc.*, **89**, 1047 (1967).
(6) D. L. Smith and J. H. Futrell, *Int. J. Mass Spectrom. Ion Phys.*, **14**, 171 (1974).
(7) (a) J. L. Franklin, J. G. Dillard, H. M. Rosenstock, J. T. Herron, K. Draxl, and F. H. Field, "Ionization Potentials, Appearance Potentials, and Heats of Formation of Gaseous Positive Ions", NSRDS-NBS 26, U.S. Government Printing Office, 1969; (b) S. E. Buttrill, Jr., A. D. Williamson, and P. LeBreton, *J. Chem. Phys.*, **62**, 1586 (1975).
(8) R. D. Smith and J. H. Futrell, *Int. J. Mass Spectrom. Ion Phys.*, **20**, 347 (1976).
(9) R. C. Dunbar, J. Shen, and G. A. Olah, *J. Am. Chem. Soc.*, **94**, 6862 (1972), and references cited therein.
(10) K. L. Rinehart, A. C. Buchholz, G. E. Van Lear, and H. L. Cantrill, *J. Am. Chem. Soc.*, **90**, 2983 (1968).
(11) R. C. Dunbar, *J. Am. Chem. Soc.*, **97**, 1382 (1975).
(12) A. Flaux, B. Wirz, and T. Gäumann, *Helv. Chim. Acta*, **57**, 708 (1974), and references cited therein.
(13) For examples of applications of the quasi-equilibrium theory of mass spectra to ion–molecule reactions, see M. L. Vestal in "Fundamental Processes in Radiation Chemistry", P. Ausloos, Ed., Interscience, New York, N.Y., 1968.

Quantitative Comparison of Theoretical Calculations with the Experimentally Determined Electron Density Distribution of Formamide

E. D. Stevens,* J. Rys, and P. Coppens

Contribution from the Department of Chemistry, State University of New York at Buffalo, Buffalo, New York 14214. *Received July 28, 1977*

Abstract: A thermally smeared theoretical electron density distribution of the formamide molecule is calculated for comparison with an experimental distribution deduced from x-ray diffraction measurements at 90 K. The theoretical density is obtained from an extended basis set wave function and smeared using the rigid body thermal motions derived from the low-temperature x-ray experiment. Agreement between theory and experiment over much of the molecule is within twice the estimated standard deviation of the experimental density. Significant differences include elongation of the experimental C–N bond peak along the bond axis, and nonbonding density peaks near the oxygen above and below the molecular plane in the experimental density. Discrepancies between theory and experiment are discussed in terms of deficiencies in the model including neglect of internal thermal motion, neglect of intermolecular interactions, lack of flexibility in the basis set, and neglect of electron correlation.

Introduction

The theoretical electron density distribution is a detailed property of a system which is sensitive to the quality of the molecular wave function. It is poorly reproduced by semiempirical or minimal basis set calculations and converges slowly to the Hartree–Fock limit as the basis set size is increased.[1,2] Since experimental electron density distributions are now available from accurate x-ray diffraction experiments, the extent to which theoretical and experimental densities agree is of interest. The agreement found for small molecules gives an indication of the reliability of experimental measurements on larger molecules for which rigorous calculations are currently impossible. Although the experimental results do not yield the wave function itself, they provide a detailed and sensitive property which any trial wave function must satisfy.

Experimental densities are smeared by thermal motion in the crystal. To compare theoretical densities with experimental measurements, we apply the thermal motion as derived from the x-ray data to the theoretical static density. This convolution removes some of the sharper features of the static density which cannot be deduced from the experimental measurements at finite resolution.

Relatively few comparisons have been made between experimental and theoretical electron density distributions.[3] Several of those published have employed limited basis sets such as the 4-31G set for tetracyanoethylene[4] and the double ζ set for thiourea,[5] which may, however, be improved by the addition of atom and bond polarization functions.[4] We have recently compared the density of the azide ion as found in NaN_3 and KN_3 with a thermally smeared large basis set theoretical density on N_3^-,[6] and report here a comparison of the experimental low-temperature density distribution of form-

0002-7863/78/1500-2324$01.00/0

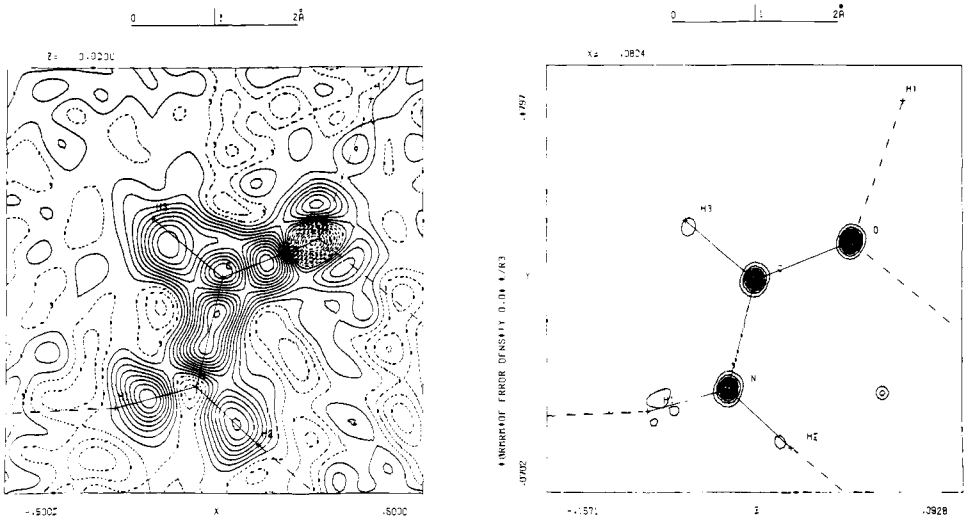

Figure 1. (a) Experimental deformation density in the plane of the formamide molecule. Contours at 0.05 e/Å^3, negative contours broken. (b) Estimated error distribution in the experimental density. Contours at 0.01 e/Å^3, lowest contour at 0.04 e/Å^3.

amide with an extended basis set ab initio theoretical calculation including rigid body thermal smearing.

Computational Methods

Experimental Densities. Details of the electron density distribution related to chemical bonding are readily visualized in a plot of the deformation density defined as

$$\Delta\rho = \rho_{obsd} - \rho_{reference} \quad (1)$$

where the reference state is the density calculated for an assembly of isolated spherical atoms placed at the nuclear positions.

The experimental density distribution has been derived from high-resolution x-ray diffraction measurements on a single crystal of formamide at 90 K. Details of the experiment are described elsewhere.[7] Since least-squares refinement of x-ray data is biased by the asphericity of the valence electron distribution, positional and thermal parameters for the C, N, and O atoms used in the reference density are obtained from a high-order refinement including only reflections with $\sin\theta/\lambda > 0.85$ Å^{-1}. The hydrogen parameters cannot be obtained from this refinement as hydrogen scattering is insufficient above the 0.85 Å^{-1} cutoff. They were therefore taken from a refinement of all data with $\sin\theta/\lambda > 0.60$ Å^{-1}. These parameters have relatively large standard deviations but the resulting bond lengths are in good agreement with those from microwave and electron diffraction results (Table I). The larger standard deviations are properly incorporated in the calculated charge density error distribution (see below). As the total density near the hydrogen is low compared with the density near the other atoms, the hydrogen-parameter standard deviations do not produce dominant features in the error map.

The resulting deformation density is plotted in Figure 1 along with the distribution of the estimated standard deviation. The reference state of the deformation density (Figure 1a) is taken as spherical Hartree–Fock atoms with positional and thermal parameters from the high-order refinement. The error distribution is relatively constant with an average value of 0.03 e/Å^3 at positions not near atomic centers or crystallographic symmetry elements. Within about 0.3 Å of the nucleus, errors in the positional and thermal parameters of the model and the overall scale factor give rise to a much larger estimated error.

Table I. Comparison of Bond Distances and Angles

	X-ray full data	X-ray high order[a]	Electron diffraction[b]	Microwave[c]
	Bond distances, Å			
C=O	1.241 (1)	1.239 (4)	1.211 (4)	1.219 (12)
C-N	1.318 (1)	1.326 (4)	1.367 (4)	1.352 (12)
C-H3	1.01 (1)	1.09 (5)	1.12[d]	1.098 (10)
N-H1	0.87 (1)	1.01 (5)	1.021 (9)[e]	1.002 (3)
N-H2	0.89 (1)	1.01 (5)	1.021[e]	1.002 (3)
	Bond Angles, deg			
N-C=O	125.0 (1)	124.9 (3)	124.9 (5)	124.7 (3)
N-C-H3	114.5 (6)	116 (3)	112.7[d]	112.7 (2)
C-N-H1	118.9 (7)	118 (3)	120.0[d]	120.0 (3)
C-N-H2	119.6 (7)	119 (3)	118.5[d]	118.5 (5)

[a] $(\sin\theta/\lambda)_{min} = 0.80$ Å^{-1} for O, N, and C parameters; 0.60 Å^{-1} for H parameters. [b] Reference 14a. [c] Reference 14b. [d] Fixed. [e] Constrained $r_{N-H1} = r_{N-H2}$.

To some extent, measurements of the intensities of elastically scattered x rays are affected by thermal diffuse scattering which can be allowed for it elastic constants are available, which is not the case for formamide. However, calculations by Helmholdt and Vos[8] indicate that the effect on low-temperature x-ray deformation densities is minor (less than 0.03 e/Å^3 for dibenzoyl and ammonium hydrogen oxalate at 110 K), except near nuclear positions.

Theoretical Densities. The theoretical deformation density of the formamide molecule was obtained from an ab initio SCF molecular orbital wave function calculated using the program HONDO[9] and an extended basis set of Gaussian orbitals. To obtain reliable theoretical densities, it has been found that large basis sets including d functions are required.[1,2] The extended set of Pople and Binkley[10] was chosen with an additional s-type function added to the hydrogens to take advantage of the shell structure of HONDO. The final (11, 5, 1/6, 1) set of primitive Gaussians contracted to a (4, 3, 1/4, 1) set is similar to the set used by Christensen et al.[11] and is expected to yield a wave function of similar quality.

The molecular geometry used for the calculation was taken from an initial high-order refinement of the x-ray data. A mirror plane was imposed on the molecule by projecting the atomic coordinates onto the best least-squares plane through the molecule. The largest deviations from the least-squares

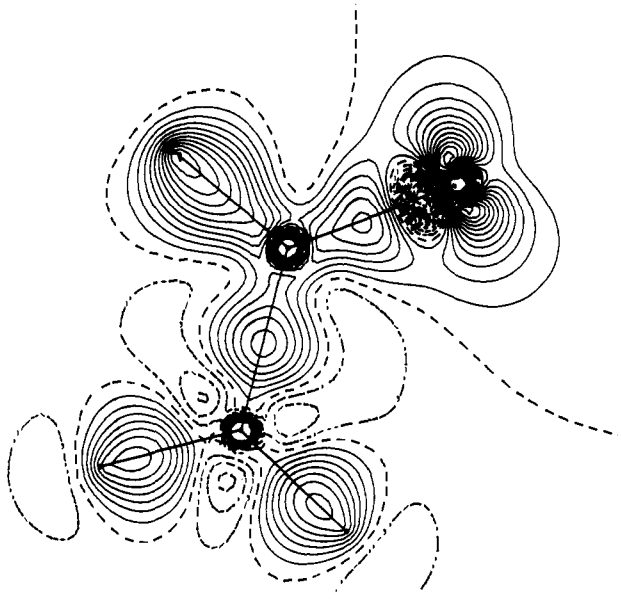

Figure 2. Static theoretical deformation density calculated for formamide. Contours at 0.10 e/Å^3, zero contour (– –), negative contour (- - - -). Large negative contours have been omitted.

plane are 0.03 (8), −0.01 (7), and 0.04 (10) Å for H1, H2, and H3, respectively. The coordinates are listed in Table II. The total energy calculated for the SCF wave function was E = −168.9689 au, slightly better than the lowest energy of −168.962 95 au reported by Christensen et al.[11]

Thermal Smearing. In order to compare the theoretical density distribution with the experiment, the effect of thermal motion on the density must be considered. In the approximation that the internal modes of vibration can be neglected, the dynamic density distribution can be obtained from a static wave function.[12] The thermal smearing is calculated from rigid-body librational and translational parameters derived from the experiment.[13] Inclusion of a screw tensor in the rigid body model did not significantly improve the agreement with the individual atomic thermal parameters. The experimental thermal motion parameters applied to the theoretical density are listed in Table III.

For most molecular solids at room temperature, displacements due to thermal motion are dominated by the large amplitude external modes. At lower temperatures, the relative importance of the internal modes increases, and the validity of the rigid-body approximation must be considered. For formamide, the contribution from the internal modes can be estimated from the gas-phase electron diffraction experiment.[14] The mean square amplitudes of motion in the gas phase at 160 °C are only 10–20% of those observed in the single-crystal x-ray experiment.[7] The largest discrepancy between the individual atomic thermal parameters in the solid and the rigid body model is an average of 0.003 Å^2 excess thermal motion observed for the hydrogen atoms due to in-plane bending. The large amplitude out of plane bending modes are absorbed by the librational motion in the rigid body model.

The rigid body thermal parameters used in the calculation are listed in Table III along with the relationship between the molecular, crystal, and inertial frames of reference. To apply thermal smearing to the theoretical density, the Fourier transform of the density is calculated analytically for each scattering vector **S** corresponding to an experimental measurement. After multiplication of the theoretical structure factors by the temperature factor, the density is obtained by an inverse Fourier transform. This procedure leads to a theoretical density which includes series termination effects caused by finite experimental resolution to exactly the same extent as the experimental density.

Table II. Atomic Coordinates Used for Theoretical Calculation (au)

Atom	X	Y	Z
O	2.190 23	0.849 44	0.000 00
N	−0.594 33	−2.427 40	0.000 00
C	0.000 00	0.000 00	0.000 00
H1	−2.440 63	−2.909 29	0.000 00
H2	0.813 54	−3.716 22	0.000 00
H3	−1.507 27	1.253 10	0.000 00

Table III. Rigid-Body Thermal Parameters Used to Smear the Theoretical Density

Translation Tensor (Å^2, Relative to Inertial Axes)		
0.0157 (19)	0.0007 (18)	−0.0023 (21)
	0.0118 (23)	0.0006 (24)
		0.0177 (34)
Libration Tensor (rad^2, Relative to Inertial Axes)		
0.0261 (26)	−0.0046 (16)	−0.0029 (17)
	0.0067 (16)	−0.0012 (12)
		0.0037 (11)
Transformation from Molecular to Crystal Axes		
0.062 30	0.000 00	0.135 45
−0.045 53	−0.030 14	0.020 94
−0.029 56	0.064 82	0.029 02
Transformation from Crystal Axes to Inertial Axes		
0.7074	−8.0859	2.5273
1.7081	−2.4828	−6.3617
3.1003	3.2129	1.4444

The low temperature and high resolution (sin θ_{max}/λ = 1.05 Å^{-1}) of the formamide experiment yield more detail in the density and allow a more critical comparison of theory and experiment than in studies with greater thermal motion or lower experimental resolution.[5]

Stereographic Projections. To display the nonbonded density features of the oxygen atom, the electron density has been plotted in stereographic projection (Figure 5). The density distribution on the surface of a hemisphere of radius 0.395 Å and centered at the oxygen atom is projected onto the plane perpendicular to the CO bond. Details of calculating the projection are described by Stevens and Coppens.[15]

Results

The static theoretical deformation density calculated for the formamide molecule is plotted in Figure 2. To minimize the effects of basis set truncation, the reference state density subtracted out in this deformation function was taken as the sum of the atomic densities calculated with the same basis set.

The dynamic theoretical deformation density calculated using rigid body thermal parameters from the experiment is plotted in Figure 3. As the flexibility of the basis set increases and thermal smearing is included, the effects of basis set truncation are likely to be less important than the deficiencies in the closed shell atomic density calculation. For this reason, spherically averaged Hartree–Fock atomic densities have been used as the reference in the dynamic deformation density.

To allow detailed comparison of the theoretical and experimental deformation densities, a second-order difference function defined by

$$\Delta(\Delta\rho) = \Delta\rho_{expt} - \Delta\rho_{theory,dynamic} \quad (2)$$

has been plotted in Figure 4. Since the reference states of both the experimental and dynamic theoretical deformation den-

Table IV. Comparison of Bond Peak Heights

Bond	Exptl	Theor
C-O	0.54 (3)	0.42
C-N	0.51 (3)	0.46
C-H3	0.44 (4)	0.61
N-H2	0.36 (4)	0.43
N-H1	0.38 (4)	0.43

sities are the same, except for small differences in positional and thermal parameters, $\Delta(\Delta\rho)$ is essentially equivalent to the difference between the total experimental and total dynamic theoretical densities. Positive regions in this map indicate excess charge in the experimental density relative to the theoretical density. To judge if the difference is significant, it is necessary to also examine the error distribution map (Figure 1b).

Peaks commonly associated with bonding and lone pair density are found in both the experimental and theoretical deformation densities. The maximum values of the bond peaks in the experimental and thermally smeared-theoretical density maps are tabulated in Table IV. The theoretical density contains two equal lone pair peaks of 0.41 e/Å^3 located in the molecular plane and 0.42 Å from the oxygen position.

The experimental map also shows density at the same positions in the molecular plane (0.23 and 0.31 e/Å^3), but the peak maxima occur at 0.52 and 0.53 e/Å^3 above and below the plane.

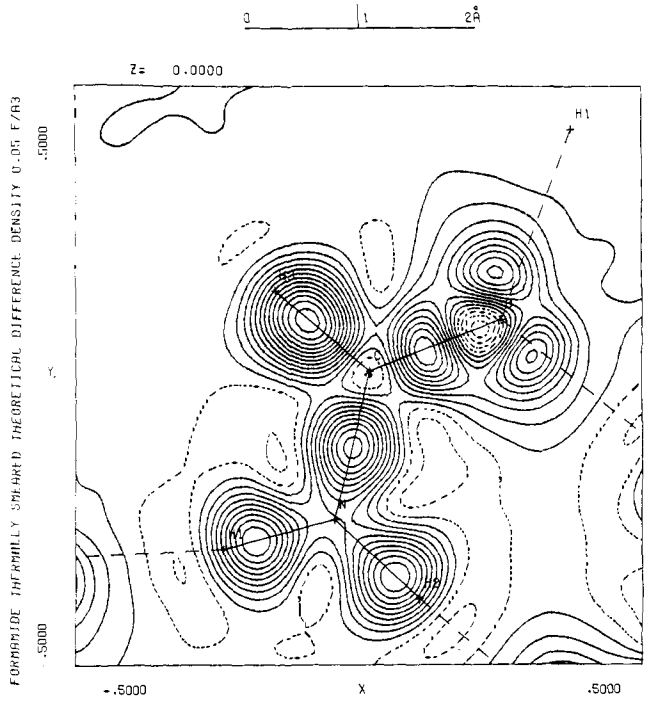

Figure 3. Dynamic theoretical deformation density calculated for formamide at 90 K. Contours as in Figure 1a.

Discussion

In much of the molecule the agreement between theory and experiment is within twice the estimated experimental standard deviation. The noise level in intermolecular regions of the experimental density indicates the estimate of 0.03 e/Å^3 for $\sigma(\Delta\rho)$ to be reasonable. The relatively large differences between theory and experiment at the nitrogen and oxygen centers are not significant because of the high $\sigma(\Delta\rho)$ at those positions.

There are, however, several regions of the molecular density where the disagreement between theory and experiment is greater than 2σ. The theoretical density is slightly lower in the CO and CN bonds and higher in the CH and NH bonds compared with the experimental density (Table IV). This can be partially attributed to the neglect of the excess thermal motion of the hydrogens compared with the rigid body model. Fitting the bond peaks with Gaussian functions, it is estimated that the heights of the CH and NH bond peaks in the smeared theoretical density would be lowered by 0.05 e/Å^3 if these internal modes were included in the thermal smearing.

Comparison of the dimensions (width at half-height) of the bond and lone pair peaks is good, though the CN and, to a lesser extent, the CO bond peaks are more extended along the bond axis in the experimental density. A similar result was found for the bond peaks of sodium and potassium azide.[6] A possible explanation for this discrepancy is that even the extended basis set employed here lacks sufficient flexibility in the bonding region. Static Hartree-Fock densities of N_2 and NCCN,[16] for example, show more elongation of the bonding peaks than the CO and CN bonds of the static formamide density.

A deficiency of the comparison is the neglect of intermolecular interactions in the theoretical calculation. The largest interactions are due to the network of hydrogen bonds formed in the solid. Calculations of the dimer-monomer density difference for formamide,[17] HF,[18] and H_2O[19] show some rearrangement of density on hydrogen bond formation throughout

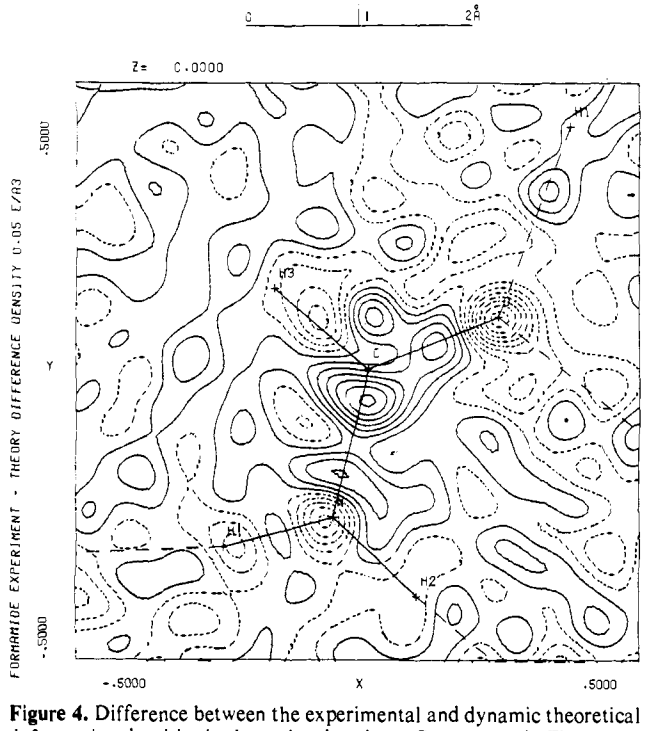

Figure 4. Difference between the experimental and dynamic theoretical deformation densities in the molecular plane. Contours as in Figure 1a.

the molecule. However, the largest effect is an increase of 0.2 e/Å^3 in the (static) density in the N-H bonds,[17] which would result in worse agreement with the experiment in the present case.

The theoretical density contains two lone pair peaks near the oxygen in the molecular plane consistent with sp^2 hybridization of the oxygen. The experimental density in this region is lower but increases to peaks above and below the plane (Figure 4). A similar result has been found in a study of the

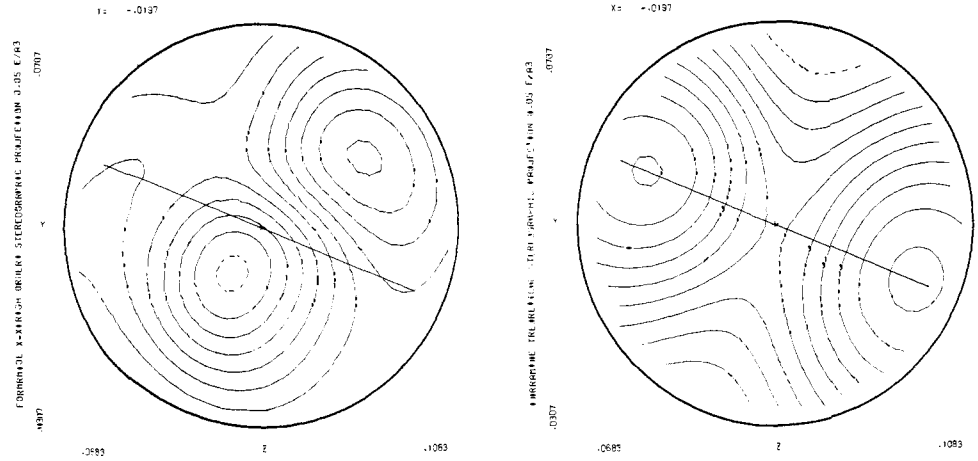

a b

Figure 5. Stereographic projection of the deformation density on the surface of a hemisphere 0.395 Å from the oxygen atom. Contours as in Figure 1a. (a) Experimental density. (b) Dynamic theoretical density.

allenedicarboxylic acid-acetamide complex,[20] for the oxygen of the acetamide but not for the allenedicarboxylic acid molecule. In going from the gas phase to the solid, the C=O and C-N bond lengths of formamide increase and decrease by 0.03 and 0.04 Å, respectively[14] (Table I) indicating a substantial decrease in bond order of the C=O bond and an increase in strength of the C-N bond. The strong hydrogen bonded network in the solid appears to increase bonding in the C-N linkage with a corresponding decrease in the C=O bond. The peaks above and below the oxygen atom evident in the experimental maps may indicate increased localization of the p_π electrons on the oxygen. This is in agreement with calculations by Johansson et al.[21] which reveal analogous changes in the π population on the formamide oxygen atom as a result of dimer formation or hydrogen bond formation with water at either the NH_2 or O sites.

In the experimental map, more density is found at 0.3-0.4 Å from the carbon and nitrogen atoms in directions away from the bonds. This increase relative to the theoretical density accounts for the rectangular shape of the C-N bond in the experimental maps. While the differences of 0.10-0.15 e/Å^3 are only marginally significant, they have also been found in the densities of NaN_3 and KN_3.[6] Calculations of the density distributions corresponding to CI wave functions for N_2 and CO show similar increases in density relative to the HF density.[22] For N_2, a maximum of 0.13 e/Å^3 in the $\rho_{CI}-\rho_{HF}$ difference density is found near the nuclei but displaced ~0.3 Å off the molecular axis. For CO, maximum differences of +0.06 and −0.04 e/Å^3 are found near the carbon and oxygen atoms, respectively, also displaced off the molecular axis. While a definitive explanation of these differences must await more rigorous calculations, the parallel with CO and N_2 strongly suggests that deficiencies of the Hartree-Fock approximation may be observable in high-accuracy experimental determinations of the electron density distribution.

In summary, we attribute small but persistent discrepancies between theory and experiment to neglect of internal modes in thermal smearing, to remaining basis set truncation, to neglect of electron correlation, and to the intermolecular interactions. Though all these effects are small compared to the main features in the deformation maps, they can in principle be evaluated theoretically. Their elucidation is clearly desirable in view of possible improvements in experimental accuracy in future studies.

Acknowledgment. Support of this work by the National Science Foundation under Grants CHE 76-13342 and CHE 76-21995 is gratefully acknowledged.

References and Notes

(1) R. F. W. Bader, *MTP Int. Rev. Sci.: Phys. Chem., Ser. 2*, **1**, 43–78 (1975).
(2) P. E. Cade, *Trans. Am. Crystallogr. Assoc.*, **8**, 1–36 (1972).
(3) P. Coppens and E. D. Stevens, *Adv. Quantum Chem.*, **10**, 1–35 (1977).
(4) H.-L. Hase, K.-W. Schulte, and A. Schweig, *Angew. Chem.*, **89**, 263–264 (1977); H.-L. Hase and A. Schweig, *ibid.*, **89**, 264–265 (1977).
(5) H.-L. Hase, H. Reitz, and A. Schweig, *Chem. Phys. Lett.*, **39**, 157–159 (1976).
(6) E. D. Stevens, J. Rys, and P. Coppens, *J. Am. Chem. Soc.*, **99**, 265–267 (1977).
(7) E. D. Stevens, *Acta Crystallogr.*, in press.
(8) R. B. Helmholdt and A. Vos, *Acta Crystallogr., Sect. A*, **33**, 38–45 (1977).
(9) M. Dupuis, J. Rys, and H. F. King, *J. Chem. Phys.*, **65**, 111–116 (1976); M. Dupuis and H. F. King, *J. Comput. Phys.*, **21**, 144–165 (1976).
(10) J. A. Pople and J. S. Binkley, *Mol. Phys.*, **29**, 599–611 (1975).
(11) D. H. Christensen, R. N. Kortzeborn, B. Bak, and J. J. Led, *J. Chem. Phys.*, **53**, 3912–3922 (1970).
(12) E. D. Stevens, J. Rys, and P. Coppens, *Acta Crystallogr., Sect. A*, **33**, 333–338 (1977).
(13) V. Schomaker and K. N. Trueblood, *Acta Crystallogr., Sect. B*, **24**, 63–76 (1968).
(14) (a) M. Kitano and K. Kuchitsu, *Bull. Chem. Soc. Jpn.*, **47**, 67–72 (1974); (b) E. Hirota, R. Sugisaki, C. J. Nielsen, and G. A. Sørensen, *J. Mol. Spectrosc.*, **49**, 251–267 (1974).
(15) E. D. Stevens and P. Coppens, *J. Cryst. Mol. Struct.*, in press.
(16) R. F. W. Bader, W. H. Henneker, and P. E. Cade, *J. Chem. Phys.*, **46**, 3341–3363 (1967); F. L. Hirshfeld, *Acta Crystallogr., Sect. B*, **27**, 769–781 (1971).
(17) M. Dreyfus, B. Maigret, and A. Pullman, *Theor. Chim. Acta*, **17**, 109–119 (1970); M. Dreyfus and A. Pullman, *ibid.*, **19**, 20–37 (1970).
(18) P. A. Kollman and L. C. Allen, *J. Chem. Phys.*, **52**, 5085–5094 (1970).
(19) S. Yamabe and K. Morokuma, *J. Am. Chem. Soc.*, **97**, 4458–4465 (1975).
(20) Z. Berkovitch-Yellin, L. Leiserowitz, and F. Nader, *Acta Crystallogr., Sect. B*, **33**, 3670–3677 (1977).
(21) A. Johansson, P. Kollman, S. Rotherberg, and J. McKelvey, *J. Am. Chem. Soc.*, **96**, 3794–3800 (1974).
(22) P. Becker, private communication; F. Grimaldi, A. Lecourt, and C. Moser, *Int. J. Quantum Chem.*, **1S**, 153 (1967).